CHEMIJA. 2017. Vol. 28. No. 2. P. 93–98

Photoelectrochemical behaviour of WO_3 and Se-WO_3 films modified with cobalt-based oxygen evolving catalyst

Simona Ostachavičiūtė*,

Agnė Šulčiūtė,

Eugenijus Valatka

Department of Physical and Inorganic Chemistry, Kaunas University of Technology, Radvilėnų Rd. 19, LT-50254 Kaunas, Lithuania

Thin films of bare and Se-containing tungsten trioxide (WO_3) on AISI304 stainless steel were prepared by electrochemical deposition using peroxy-tungstate solutions. Cobalt-phosphate catalyst was photochemically deposited onto the surface of semiconductor particles in order to enhance their activity towards the oxygen evolution reaction. The photoelectrochemical properties of as-prepared electrodes were investigated in neutral 0.1 M phosphate buffer solutions. The voltammetric characteristics revealed that the presence of cobalt-based catalyst effectively changes the photoelectrocatalytic activity of WO_3 and Se-WO_3 particles.

Keywords: tungsten trioxide (WO_3), mixed tungsten trioxide–selenium film, oxygen evolution catalyst, electrodeposition, stainless steel

INTRODUCTION

As fossil fuel reserves are depleting and environmental issues are getting more important every day, heterogeneous photo(electro)catalysis remains an attractive alternative in search of ways to utilize clean energy sources. It is constantly tested for various applications: degradation of organic pollutants [1, 2], reduction of CO_2 [3, 4], hydrogen and oxygen production through photocatalytic water-splitting [5–9], photocatalytic synthesis of organic substances [10–12], even inactivation of microorganisms [13]. Various semiconductor photocatalysts were studied for such purposes with the focus on the oxide-based ones, such as TiO_2 [14–16], WO_3 [17–19], ZnO [20] and Fe_2O_3 [21, 22], due to their stability, low cost and higher activity. However, there is still a need for the stable highly photosensitive materials with improved spectral response spanning toward the visible region, and plenty of strategies to achieve this goal can be applied [23]. They include sensitization, photocatalyst morphology modification, doping, creating heterostructures or composite materials, etc.

Since the oxygen evolution reaction (OER) requires the removal of four protons and four electrons and the formation of oxygen–oxygen double bond, it is considered the main obstacle in the realization of photoelectrochemical water splitting [24, 25]. In 2008, Nocera et al. [26] reported for the first time that a highly active water oxidation catalyst can be obtained by the electrolysis of Co^{2+} salts in a neutral phosphate electrolyte using ITO glass as a support. The as-deposited cobalt-phosphate compound (termed Co–P_i) has been proved to be very active in neutral pH solutions [27–31]. It also has been demonstrated that a Co–P_i oxygen evolving catalyst can be coupled with semiconductors via electrochemical [26–32] or photochemical [33, 34] routes and enhance the efficiency of photoelectrochemical water splitting [32–35]. Structural studies of the cobalt-phosphate oxygen evolving catalyst suggest [28, 36] that Co–P_i is composed of bis-μ-oxo/hydroxo-linked Co ions and support a molecular cobaltate cluster (MCC) model. According to this model the Co-oxo/hydroxo clusters possess the same structural motif found in the extended planes of cobaltates – edge sharing CoO_6 octahedra – but have molecular dimensions. It has been suggested that the molecular dimensions of the clusters found in Co–P_i may be essential for OER catalysis. Using synchrotron-based X-ray grazing incidence diffraction, Nocera and Liu [36] showed that these cobaltate clusters arrange into nanoparticles, whereas a conventional X-ray diffraction analysis shows catalyst films to be amorphous.

We have previously synthesized and studied bare and selenium containing tungsten trioxide (WO_3 and Se-WO_3) thin films on AISI304 type stainless steel [37]. The obtained

* Corresponding author. E-mail: simona.ostachaviciute@ktu.lt

films were characterized by X-ray diffraction, photoelectron spectroscopy, scanning electron microscopy, thermal and photovoltammetry analyses. It has been established that the presence of selenium enhances the IPCE for a WO_3 photoanode in a 0.1 M K_2SO_4 supporting electrolyte. **The aim of this work** was to modify these films on AISI304 type stainless steel with a cobalt-based OER catalyst and to study their photoelectrochemical properties in aqueous solutions.

MATERIALS AND METHODS

Bare and selenium-containing tungsten trioxide coatings (denoted as WO_3 and Se-WO_3 throughout this paper) on stainless steel were prepared by electrochemical deposition using a standard three electrode cell. AISI304 stainless steel plates 0.5 mm thick were used as a support. According to the manufacturer the composition of stainless steel is as follows (wt.%): C, 0.08; Cr, 18–20; Ni, 8–10.5; Mn, 2.0; Si, 1.0; P, 0.045; S, 0.03; Fe, the remaining amount. All solutions were prepared with doubly distilled water and analytical grade reagents. Sodium tungstate ($Na_2WO_4 \cdot 2H_2O$, purity >99.7%) was obtained from Reachim (Russia) and used as received. The electrolyte itself was prepared according to the following procedure. First, a sodium tungstate solution was mixed with hydrogen peroxide (H_2O_2, 30%, Lach-Ner, Czech Republic). Afterwards, selenious and nitric acids (HNO_3, 65%, Penta, Czech Republic) were added to the solution containing a tungsten(VI)-peroxo complex. Only freshly prepared solutions were used for the measurements. All solutions were not deaerated during the experimental runs. All measurements were carried out at an ambient temperature (291 K). The as-deposited samples were thermally treated under air atmosphere at 673 K for 1 h. The most uniform and stable films are obtained at –0.35 V after 20 min of electrolysis in a 0.1 M Na_2WO_4 + 0.1 M H_2O_2 + 0.3 M HNO_3 electrolyte for WO_3 and a 0.1 M Na_2WO_4 + 0.1 M H_2O_2 + 0.3 M HNO_3 + 0.01 M H_2SeO_3 electrolyte for Se-WO_3 films, respectively.

In order to avoid the harmful effect of +1.1 V potential on the structure of as-prepared WO_3 and Se-WO_3 thin films, a photochemical method was employed for further modification with a Co–P_i catalyst. For this purpose, the photoanode was immersed in the 0.1 M phosphate solution (pH 7) containing 0.5 mM $Co(NO_3)_2$ and illuminated for 5–40 minutes with a 400 W high pressure metal halogen lamp (Philips 400/30S).

The photoactivity of the prepared electrodes was investigated using photovoltammetric methods. The electrochemical measurements in the dark and under UV irradiation were performed by a computer-controlled Autolab PGSTAT12 (Ecochemie, The Netherlands) potentiostat/galvanostat. The GPES® 4.9 software was used for the collection and treatment of the experimental data. A photoelectrochemical quartz cell was employed. The electrolyte volume was 100 mL. Throughout the paper all potentials are referred to an Ag, $AgCl|KCl_{(sat)}$ reference electrode. A platinum wire was used as a counter electrode. A 0.1 M potassium phosphate solution (pH 7) was used as a supporting electrolyte. The back side of the working electrode was insulated with the epoxy resin in order to eliminate its contribution to the dark current. A General Electric F8W/BLB lamp was placed at a distance of 2 cm from the WO_3 or Se-WO_3 electrode and was used as an UV radiation source. The lamp emits mainly in the 315–400 nm range, the peak wavelength λ_{max} being at 366 nm. The average power density at 366 nm was determined to be 1.8 mW cm^{-2}.

The incident photon-to-current efficiency (IPCE) value of a photoelectrode was calculated using the following expression [38]:

$$\mathrm{IPCE}(\%) = 100\frac{1240 j_{ph}}{\lambda P} \cdot \tag{1}$$

Here j_{ph} is the photocurrent density in mA · cm^{-2}, λ is the wavelength of the incident light in nanometers (the value used in this study was 366 nm), P is the incident light intensity in mW · cm^{-2}.

The photoconversion efficiency (light energy to chemical energy conversion) ε was calculated as follows [35]:

$$\varepsilon = \frac{(1.23 - E_{eksp}) j_{ph}}{P} \cdot \tag{2}$$

Here j_{ph} is the photocurrent density (mA · cm^{-2}) obtained under the applied bias E_{eksp} (V), and P is the incident light intensity in mW · cm^{-2}.

RESULTS AND DISCUSSION

Photoelectrochemical behaviour of bare WO_3 and Se-WO_3 films

The photoelectrochemical behaviour of WO_3 and Se-WO_3 electrodes in the 0.1 M phosphate buffer (pH 7) was determined from the current–potential curves obtained in the dark and under UV irradiation (Fig. 1). The potential was swept from 0 to 1 V at 10 mV · s^{-1}. The behaviour of both electrodes is characteristic of the n-type semiconductor [39]. The observed anodic photocurrent can be related to the generation of hydroxyl radicals (•OH) and other oxidation products (e.g. H_2O_2) at the surface of WO_3 or Se-WO_3 electrodes [40]. In the insets of Fig. 1 the squares of photocurrent densities (j_{ph}^2) with respect to the applied potential (E) are plotted. These plots, according to the Gartner-Butler model [41], can be used to determine the presence of the depletion layer, which facilitates the separation of photogenerated holes and electrons. The depletion layer forms upon contact with an electrolyte when thick and continuous films are used. It results in linear rising parts of the plots j_{ph}^2 versus E, which can be observed in the inset of Fig. 1 (1). The obtained results also showed that the Se-containing tungsten oxide electrode generates higher photocurrent than bare WO_3 (Fig. 1).

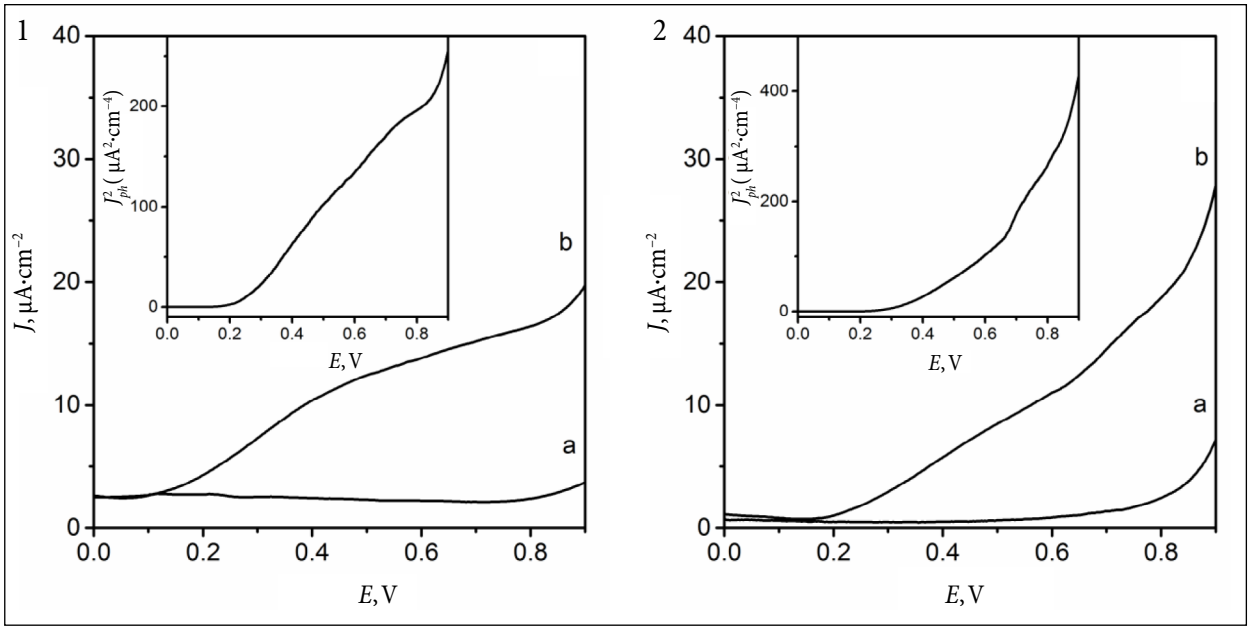

Fig. 1. Characteristic voltammograms in the dark (a) and under UV (b) illumination of WO_3 (1) and Se-WO_3 (2) electrodes in 0.10.1 M phosphate buffer (pH 7). Potential scan rate $v = 10$ mV · s^{-1}. Insets: plots of the square of photocurrent density (j_{ph}^2) with respect to the applied potential (E)

Photoelectrochemical properties of WO_3/Co–P_i and Se-WO_3/Co–P_i films

The Co–P_i oxygen evolving catalyst was formed on WO_3 and Se-WO_3 films via photochemical deposition. The amount of deposited Co–P_i was not quantitatively accounted, since the main object of this experimental part was to evaluate the synthesis time effect on the photoelectrochemical properties of tungsten oxide films.

Voltammograms of the prepared photoanodes (Figs. 2,3) in the dark were obtained to evaluate the effect of the Co–P_i layer on electrochemical oxygen evolution. The results demonstrate that the presence of the oxygen evolving catalyst shifted the onset potential for this reaction to more negative potentials by approximately 600 mV. Similar results were presented by other researchers [32]. When the synthesis duration of the Co–P_i layer reached 40 minutes, the profile

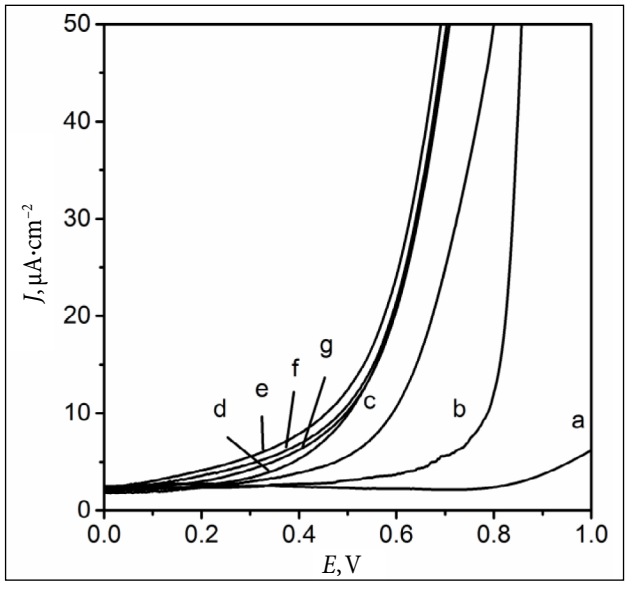

Fig. 2. Characteristic voltammograms in the dark of WO_3 (a) and WO_3/Co–P_i (b–g) films on AISI304 stainless steel in 0.1 M phosphate buffer (pH 7). Potential scan rate $v = 10$ mV · s^{-1}. The duration of Co–P_i catalyst deposition (min): b – 10, c – 20, d – 30, e – 40, f – 50, g – 60

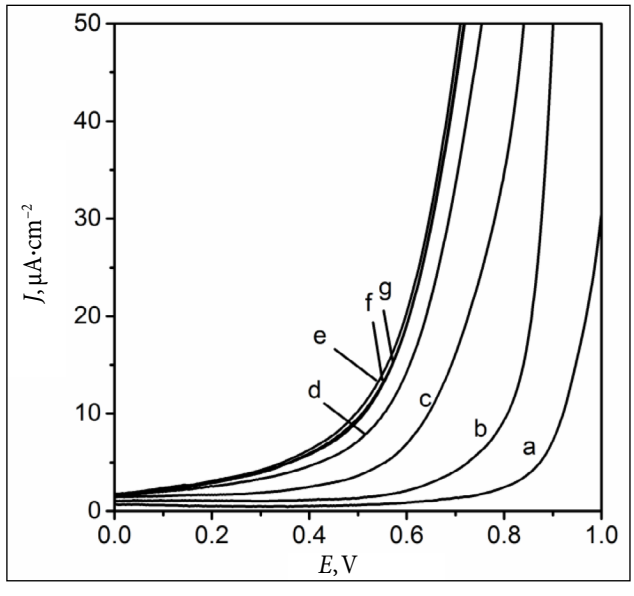

Fig. 3. Characteristic voltammograms in the dark of Se-WO_3 (a) and Se-WO_3/Co–P_i (b–g) films on AISI304 stainless steel in 0.1 M phosphate buffer (pH 7). Potential scan rate $v = 10$ mV · s^{-1}. The duration of Co–P_i catalyst deposition (min): b – 10, c – 20, d – 30, e – 40, f – 50, g – 60

of anodic current reached its stable position, thus implying the full coverage of the photoanode with the Co–P_i catalyst.

It was established that the optimal duration of the Co–P_i synthesis was 10 minutes, because both WO_3/Co–P_i and Se-WO_3/Co–P_i photoanodes generated the highest values of photocurrent density if prepared under these conditions (Figs. 4, 5). The experimental data also indicated the shift in the photocurrent onset by 0.08–0.12 V towards more negative potentials for the photoanodes coupled with the Co–P_i layer. This reveals that the layer of Co–P_i reduces the recombination rates of the photogenerated charge carriers near the flat band potential region [32].

Figure 6 presents the calculated values of IPCE (incident photon-to-current efficiency) (Eq. 1) and photoconversion efficiency ε (Eq. 2) of bare and selenium containing WO_3 catalysts in comparison with the same catalysts modified with the Co–P_i layer. The IPCE values highly depend on the supporting electrolyte. When the phosphate buffer was used, the incident photon-to-current efficiency for WO_3 and Se-WO_3 electrodes was ~2 times smaller than

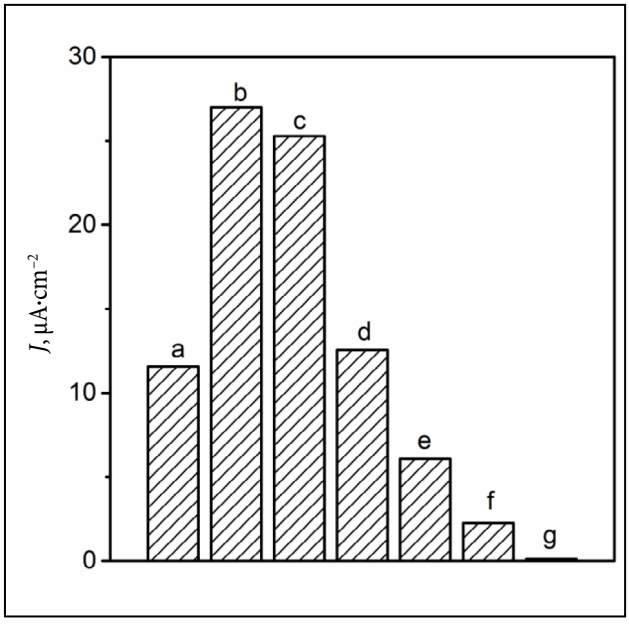

Fig. 4. Photocurrent density at +0.6 V bias for WO_3 (a) and WO_3/Co–P_i (b–g) films on AISI304 stainless steel in 0.1 M phosphate buffer (pH 7). The duration of Co–P_i catalyst deposition (min): b – 10, c – 20, d – 30, e – 40, f – 50, g – 60

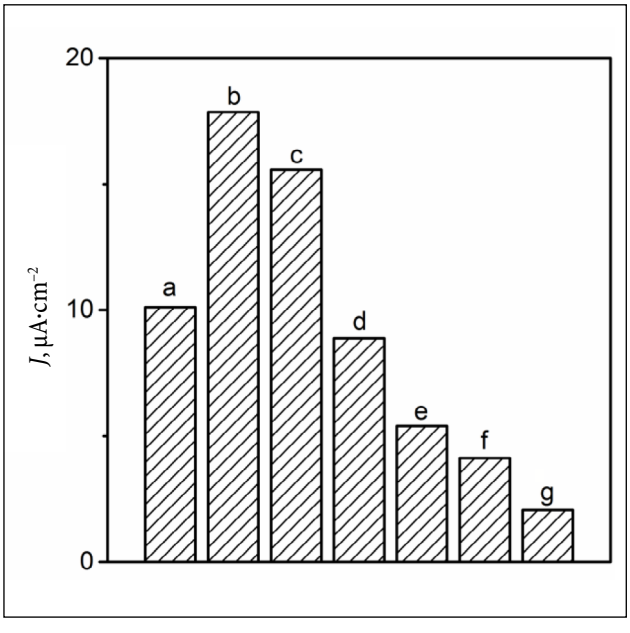

Fig. 5. Photocurrent density at +0.6 V bias for Se-WO_3 (a) and Se-WO_3/Co–P_i (b–g) films on AISI304 stainless steel in 0.1 M phosphate buffer (pH 7). The duration of Co–P_i catalyst deposition (min): b – 10, c – 20, d – 30, e – 40, f – 50, g – 60

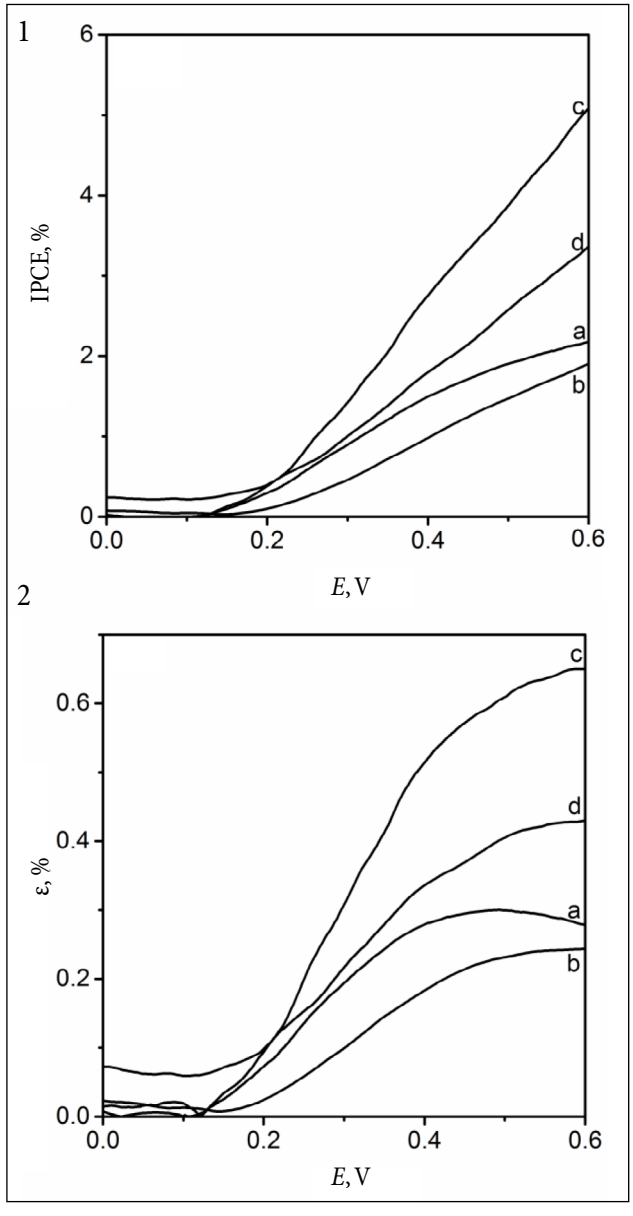

Fig. 6. The incident photon-to-current efficiency (IPCE) (1) and photoconversion efficiency values (2) for WO_3 (a), Se-WO_3 (b), WO_3/Co–P_i (c) and Se-WO_3/Co–P_i (d) films on AISI304 steel in 0.1 M phosphate buffer as a function of bias. The duration of Co–P_i catalyst deposition 10 min

it was previously determined using K_2SO_4 [37]. It is a result of strong phosphate anions adsorption on the surface of oxides, which leads to the blockage of the active centers of catalysts, thereby reducing the efficiency of photoelectrochemical processes [42]. The Co–P_i layer improved the activity of both bare and selenium-containing tungsten oxide catalysts. The WO_3/Co–P_i electrode was the most active (IPCE ~5.2%).

The calculated photoconversion efficiency ε (Fig. 6 (2)) shows that WO_3/Co–P_i has the most favourable activity (ε = 0.65%) toward photoelectrochemical water splitting.

In order to investigate the stability of photocurrent in the phosphate buffer over a prolonged irradiation time, the chronoamperometric curves were recorded using WO_3, Se-WO_3, WO_3/Co–P_i and Se-WO_3/Co–P_i electrodes (Fig. 7). It was established that for both electrodes the photocurrents decline immediately within the first 2 min. Such a complex behaviour of the studied films under UV irradiation is apparently due to the interplay of various processes occurring on the surface of the electrode. First of all, it should be noted that the chemical dissolution of WO_3 in the neutral solution takes place [43]. It is known that the chemical dissolution is not as severe as photodissolution [32]. In addition, the peroxo species are formed on the surface of WO_3 upon irradiation [44, 45]. The subsequent formation of tungsten–peroxo species leads to the loss of photoactivity. The dissolution rate induced by surface-bound peroxo species may be minimized by using acidic solutions. However, in the acidic medium Co–P_i catalyst is unstable. On the other hand, the formation of peroxo species can be prevented by the presence of the Co–P_i catalyst.

CONCLUSIONS

The nanosized WO_3 and Se-WO_3 films on AISI304 type steel were prepared by electrochemical deposition and their surface was modified with the Co–P_i catalyst via a photochemical route in order to study its influence on the photovoltammetric characteristics of electrodes. The obtained results show that the photo-assisted deposition of the Co–P_i catalyst significantly influences the photoelectrochemical activity of both films. The presence of the Co–P_i catalyst shifted the onset potential for O_2 evolution in the dark by approximately 0.6 V as compared to the bare and selenium containing WO_3. Similarly, the photocurrent onset potential was shifted by 0.1 V. It was determined that the optimum amount of the catalyst exists for the enhancement of photocurrents. The maximum value of photoconversion efficiency was determined to be 0.65% at 0.4 V for the WO_3/Co–P_i electrode.

Received 28 February 2017
Accepted 1 March 2017

References

1. R. T. Koodali, D. Zhao, *Energy Environ. Sci.*, **3(5)**, 608 (2010).
2. G. Rammohan, M. N. Nadagouda, *Curr. Org. Chem.*, **17(20)**, 2338 (2013).
3. J. Schneider, H. F. Jia, J. T. Muckerman, E. Fujita, *Chem. Soc. Rev.*, **41(6)**, 2036 (2012).
4. A. Dhakshinamoorthy, S. Navalon, A. Corma, H. Garcia, *Energy Environ. Sci.*, **5(11)**, 9217 (2012).
5. R. Abe, *J. Photochem. Photobiol., C*, **11(4)**, 179 (2010).
6. D. W. Jing, L. J. Guo, L. A. Zhao, et al., *Int. J. Hydrogen Energy*, **35(13)**, 7087 (2010).
7. H. H. Yang, L. J. Guo, W. Yan, H. T. Liu, *J. Power Sources*, **159(2)**, 1305 (2006).
8. K. Maeda, *J. Photochem. Photobiol., C*, **12(4)**, 237 (2011).
9. H. M. Chen, C. K. Chen, R. S. Liu, et al., *Chem. Soc. Rev.*, **41(17)**, 5654 (2012).
10. F. Bi, M. F. Ehsan, W. Liu, T. He, *Chin. J. Chem.*, **33(1)**, 112 (2015).
11. A. Hameed, I. M. I. Ismail, M. Aslam, M. A. Gondal, *Appl. Catal., A*, **470**, 327 (2014).
12. L. Yuliati, H. Yoshida, *Chem. Soc. Rev.*, **37(8)**, 1592 (2008).
13. S. Noimark, C. W. Dunnill, I. P. Parkin, *Adv. Drug Delivery Rev.*, **65(4)**, 570 (2013).
14. H. Park, Y. Park, W. Kim, W. Choi, *J. Photochem. Photobiol., C*, **15**, 1 (2013).
15. K. Nakata, A. Fujishima, *J. Photochem. Photobiol., C*, **13(3)**, 169 (2012).
16. M. D. Hernandez-Alonso, F. Fresno, S. Suarez, J. M. Coronado, *Energy Environ. Sci.*, **2(12)**, 1231 (2009).
17. C. A. Bignozzi, S. Caramori, V. Cristino, et al., *Chem. Soc. Rev.*, **42(6)**, 2228 (2013).
18. H. Tong, S. X. Ouyang, Y. P. Bi, et al., *Adv. Mater.*, **24(2)**, 229 (2012).
19. X. Liu, F. Y. Wang, Q. Wang, *Phys. Chem. Chem. Phys.*, **14(22)**, 7894 (2012).
20. M. Y. Guo, M. K. Fung, F. Fang, et al., *J. Alloys Compd.*, **509(4)**, 1328 (2011).
21. M. Barroso, S. R. Pendlebury, A. J. Cowan, J. R. Durrant, *Chem. Sci.*, **4(7)**, 2724 (2013).

22. D. A. Wheeler, G. M. Wang, Y. C. Ling, Y. Li, J. Z. Zhang, *Energy Environ. Sci.*, **5(5)**, 6682 (2012).
23. A. B. Djurisic, Y. H. Leung, A. M. C. Ng, *Mater. Horiz.*, **1(4)**, 400 (2014).
24. I. Katsounaros, S. Cherevko, A. R. Zeradjanin, K. J. J. Mayrhofer, *Angew. Chem., Int. Ed.*, **53(1)**, 102 (2014).
25. L. Trotochaud, S. W. Boettcher, *Scr. Mater.*, **74**, 25 (2014).
26. M. W. Kanan, D. G. Nocera, *Science*, **321(5892)**, 1072 (2008).
27. D. K. Bediako, C. Costentin, E. C. Jones, D. G. Nocera, J. M. Saveant, *J. Am. Chem. Soc.*, **135(28)**, 10492 (2013).
28. M. W. Kanan, J. Yano, Y. Surendranath, et al., *J. Am. Chem. Soc.*, **132(39)**, 13692 (2010).
29. Y. Surendranath, M. Dinca, D. G. Nocera, *J. Am. Chem. Soc.*, **131(7)**, 2615 (2009).
30. Y. Surendranath, M. W. Kanan, D. G. Nocera, *J. Am. Chem. Soc.*, **132(46)**, 16501 (2010).
31. Y. Surendranath, D. A. Lutterman, Y. Liu, D. G. Nocera, *J. Am. Chem. Soc.*, **134(14)**, 6326 (2012).
32. J. A. Seabold, K. S. Choi, *Chem. Mater.*, **23(5)**, 1105 (2011).
33. E. M. P. Steinmiller, K. S. Choi, *Proc. Natl. Acad. Sci. USA*, **106(49)**, 20633 (2009).
34. R. S. Khnayzer, M. W. Mara, J. Huang, et al., *ACS Catal.*, **2(10)**, 2150 (2012).
35. Q. Liu, Q. P. Chen, J. Bai, et al., *J. Solid State Electrochem.*, **18(1)**, 157 (2014).
36. Y. Liu, D. G. Nocera, *J. Phys. Chem. C*, **118(30)**, 17060 (2014).
37. S. Ostachaviciute, J. Baltrusaitis, E. Valatka, *J. Appl. Electrochem.*, **40(7)**, 1337 (2010).
38. J. Georgieva, S. Armyanov, E. Valova, I. Poulios, S. Sotiropoulos, *Electrochem. Commun.*, **9(3)**, 365 (2007).
39. M. Gratzel, *Heterogeneous Photochemical Electron Transfer*, CRC Press, Boca Raton (1989).
40. M. R. Hoffmann, S. T. Martin, W. Choi, D. W. Bahnemann, *Chem. Rev.* (*Washington, DC, U. S.*), **95(1)**, 69 (1995).
41. J. Georgieva, S. Armyanov, E. Valova, et al., *J. Electroanal. Chem.*, **585(1)**, 35 (2005).
42. Ž. Kulėšius, Ph. D. Thesis, Kaunas University of Technology (2008).
43. R. A. Carcel, L. Andronic, A. Duta, *Mater. Charact.*, **70**, 68 (2012).
44. J. Augustynski, R. Solarska, H. Hagemann, C. Santato, *Solar Hydrogen and Nanotechnology*, San Diego (2006).
45. M. Gratzel, Y. Oosawa, *J. Chem. Soc., Chem. Commun.*, **24**, 1629 (1984).

Simona Ostachavičiūtė, Agnė Šulčiūtė, Eugenijus Valatka

WO_3 IR Se-WO_3 DANGŲ, MODIFIKUOTŲ KOBALTO TURINČIU DEGUONIES IŠSISKYRIMO KATALIZATORIUMI, FOTOELEKTROCHEMINĖ ELGSENA

S a n t r a u k a

Darbo metu elektrocheminiu metodu suformuotos WO_3 ir Se-WO_3 dangos ant AISI304 markės nerūdijančiojo plieno ir modifikuotos kobalto turinčiu deguonies išsiskyrimo katalizatoriumi Co–P_i.

Tiriant gautųjų dangų savybes 0,1 mol/l fosfatiniame buferiniame tirpale (pH = 7) nustatyta, kad naudojant WO_3/Co–P_i ir Se-WO_3/Co–P_i dangas deguonies išsiskyrimo reakcijos potencialas pasislenka 600 mV neigiamesnių potencialų kryptimi, palyginti su nemodifikuotomis dangomis. Taip pat pastebėtas modifikuotų oksidinių dangų fotoelektrocheminio aktyvumo padidėjimas, palyginti su nemodifikuotomis WO_3 ir Se-WO_3 dangomis. Modifikuotų fotoanodų generuojamos fotosrovės atsiranda prie 0,08–0,12 V neigiamesnių potencialų. Nustatytos optimalios sąlygos kobalto turinčio deguonies išsiskyrimo katalizatoriaus sluoksniui formuoti: efektyviausi pasirodė WO_3/Co–P_i ir Se-WO_3/Co–P_i elektrodai, kai Co–P_i katalizatoriaus fotocheminės sintezės trukmė 10 min. WO_3/Co–P_i elektrodui suteikus 0,4 V potencialą maksimalus vandens fotokonversijos į elementus efektyvumas siekia 0,67 %.